Insight into the nitrogen-vacancy center formation in type-Ib diamond by irradiation and annealing approach

Taiqiao Liu[1,6]**, Fanglin Lyu**[2,6]**, Tian Shao**[2]**, Diwei Zou**[1]**, Wei Shen**[1,*]**, Yuzheng Guo**[3]**, Yuan Zhong**[2]**, Chaoyang Chen**[2]**, Liangchen Yi**[4]**, Zhaofu Zhang**[1,5,*] **and Andy H Shen**[2,*]

[1] The Institute of Technological Sciences, Wuhan University, Wuhan 430072, People's Republic of China
[2] Gemmological Institute, China University of Geosciences, Wuhan 430074, People's Republic of China
[3] School of Electrical Engineering and Automation, Wuhan University, Wuhan 430072, People's Republic of China
[4] Zhongnan Diamond Company, Nanyang 473264, People's Republic of China
[5] Hubei Key Laboratory of Electronic Manufacturing and Packaging Integration, Wuhan University, Wuhan 430072, People's Republic of China

E-mail: zhaofuzhang@whu.edu.cn, wei_shen_@whu.edu.cn and shenxt@cug.edu.cn

CrossMark

Abstract

Comprehending the microscopic formation of nitrogen vacancy (NV) centers in nitrogen-doped diamonds is crucial for enhancing the controllable preparation of NV centers and quantum applications. Irradiation followed by annealing simulations for a type-Ib diamond with a 900 ppm concentration of isolated nitrogen is conducted along different orientations and at different annealing temperatures. In these simulations, molecular dynamics (MD) with smoothly connected potential functions are implemented. MD simulations revealed the dynamic formation process of the NV center, which was subsequently verified by first-principles calculations and experiments. The results indicate that vacancies undergo one or multiple migrations by exchanging sites with neighboring atoms. There are three mechanisms for the formation of NV centers: direct irradiation-induced NV formation, irradiation with further annealing to form NV and vacancy migration (VM) during the annealing process. Furthermore, the results show that both VM and NV center formations are affected by orientations. This study clarifies the formation of NV centers across multiple scales and provides a solid foundation for the targeted preparation of NV centers.

Supplementary material for this article is available online

Keywords: diamond, NV center, irradiation, annealing, molecular dynamics

---

[6] These authors contributed equally to this study.
[*] Authors to whom any correspondence should be addressed.

1. Introduction

Nitrogen vacancy (NV) center in diamonds is a complex defect composed of a carbon vacancy and a neighboring substitutional nitrogen (N) atom [1]. It can achieve nanometer-level spatial resolution [2] and high sensitivity at the picotesla level [3] in promising applications such as quantum sensing, quantum computing [4, 5], biofluorescent labeling [6, 7], temperature sensing [8, 9] and magnetic field measurements [10, 11]. Quantum sensing and computing require shallow NV centers within several nanometers, while NV centers at slightly deeper depths, approximately 25 nm, help mitigate the broadening of nuclear magnetic resonance (NMR) signals caused by spin dispersion [12–14]. In the application of biological imaging, the fluorescence intensity of fluorescent nanodiamonds is relatively low, mainly due to the smaller absorption cross-section of NV⁻ centers, which can be improved by increasing the density of NV⁻ centers [15, 16]. Thus, managing the preparation of NV centers holds significant importance.

NV centers in diamond can be generated both during the growth process by chemical vapor deposition [17], high-energy particle irradiation, ion implantation and femtosecond laser irradiation, followed by subsequent annealing [18–20]. The combination of irradiation and annealing attracts the most interest, for its advantages in producing NVs of high concentration and large depth [21–23]. The irradiation-annealing approach usually begins by irradiating a diamond with an accelerated electron or neutron beam to introduce vacancies that migrate during the annealing process [23]. The yield of NV centers highly depends on the energy of incident particles, the annealing temperature, the concentration of isolated nitrogen impurity atoms in diamond and the vacancy concentration after irradiation.

High-energy particle irradiation and high-temperature annealing approaches are advantageous for NV center formation [24], although exceedingly high temperatures can degrade NV yield. Experimental results show that vacancy migration (VM) usually begins at around 873 K [25, 26]. Annealing at temperatures between 973 and 1173 K allows vacancies to move freely within a certain distance, seeking nitrogen atoms to form NV centers with a concentration lower than 5 ppm [27]. Increasing the annealing temperature to 1073–1173 K causes vacancies to migrate faster and farther, enabling them to be more easily grabbed by the neighboring substitutional nitrogen atoms, thereby allowing the NV center concentration to reach saturation [28]. Regarding nitrogen concentration, in millimeter-level single-crystal diamonds with a nitrogen concentration of 26 ppm, irradiation with high-energy electrons and *in situ* subsequent annealing resulted in approximately 5 ppm NV⁻ centers [22]. NV centers with a concentration of 3 ppm can be produced by ultra-high energy (155 MeV) electron irradiation in diamonds containing less than 200 ppm nitrogen [18]. In diamonds with 100 ppm nitrogen, at most 17.5% of the nitrogen was employed to produce NV centers, yielding about 17.5 ppm NV⁻ centers [23]. Simultaneous electron irradiation and annealing can increase the formation efficiency of the NV center by 117% [21]. To summarize, there have been numerous experimental studies on the preparation of NV centers by post-irradiation annealing, but the current experiments are unable to achieve controllable preparation of NV centers. Due to the complexity, high cost of experiments and the lack of theoretical support, it is challenging to optimize the process parameters experimentally.

However, few investigations have extensively studied the mechanisms of NV center formation at the atomic level. Mainwood [29] used semi-empirical molecular orbital techniques to analyze the structure and features of aggregated nitrogen atoms in diamond. Deák *et al* [30] calculated the charge transition levels of substitutional nitrogen, vacancies and related point defects using density functional theory (DFT) simulations. It was also demonstrated that NV centers can be formed with nitrogen in the split-interstitial sites [31]. Molecular dynamics (MD) simulations of irradiation have been used to demonstrate the mechanism of irradiation damage in pure diamond [32–34], silicon carbide [35], etc. However, the insightful understanding of the microscopic mechanism of the NV center preparation process still lacks clarity at the atomic scale.

Compared with previous studies, herein, we focus on revealing the microscopic mechanism and defect evolution process of NV centers prepared by irradiation-annealing of type-Ib diamond from a multi-scale perspective combining MD simulation, first-principles calculation and experimental verification. Different incident directions ([111], [110] and [100]) and annealing temperatures (973, 1073 and 1173 K) are considered. Our research indicates that NV centers can be formed by three microscopic mechanisms, namely irradiation-induced NV formation (INF), irradiation with further annealing (IFA) and VM towards nitrogen to form NV centers, respectively. To further reinforce the reliability of our MD findings, DFT calculations and physical experiments were performed, consistently producing results that validated the MD simulations. These results enhance the understanding of the formation mechanism of NV centers and provide a strong basis for the controllable preparation of NV centers, as well as for further research in the field of quantum information science.

2. Theory and experimental methods

2.1. Interaction potential

The Ziegler–Biersack–Littmark (ZBL) potential [36] and the Tersoff potential [37] were used to describe short-range interactions and long-range interactions between atoms, respectively. This has also been used to simulate the behavior of nitrogen ions implanted into diamond [38, 39]. The expressions for the potential functions are included in the Supplementary Information (SI) file. As shown in figure 1, we pioneeringly created a smooth connection between the Tersoff and ZBL potential functions (Tersoff–ZBL), with parameters shown in table S1. Note that the r_C and A_F for N–C and N–N interactions were originally derived in this study. Other parameters were from the reported references, for example, the interaction potential for C–C was from [37], the interaction potential
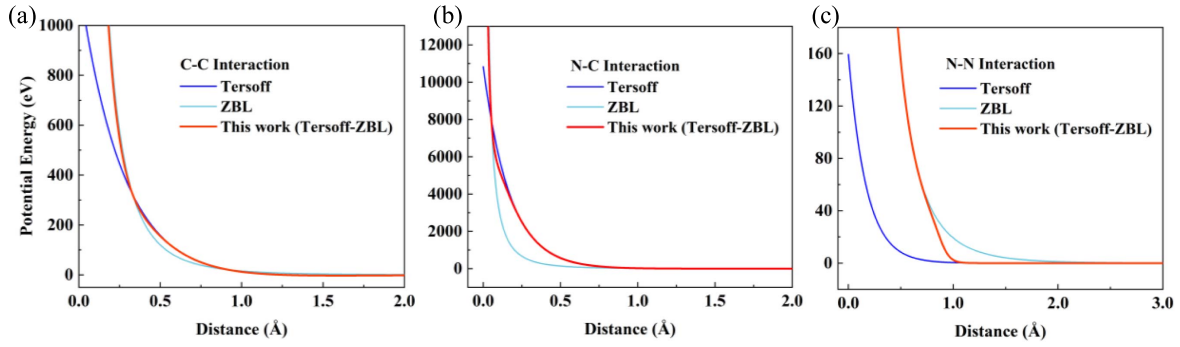
Figure 1. Interaction potential energy as a function of distance for (a) C–C, (b) N–C and (c) N–N interactions, respectively. Tersoff and ZBL potentials are connected by a Fermi-like function.

for N–C was from [40, 41], the N–N potential was calculated in [42] and the r_C and A_F for C–C was from [27].

The formation energy can be calculated using the following formula [43, 44].

For the vacancy and interstitial,

$$E_{v/i}\left(S\right) = E_d - E_{ideal} \pm n_d\mu_d. \tag{1}$$

For the substitutional,

$$E_f(S) = E_d - \left(E_{ideal} - \mu_C + \mu_N\right), \tag{2}$$

where E_{ideal} and E_d are the total energies of the ideal and defective diamond supercells, respectively. μ_C and μ_N are chemical potentials, which are approximated as the nominalized total energy of atoms in diamond and nitrogen molecules. μ_d is the chemical potential of the removed (+) or added (−) elements required to create n_d vacancies or interstitials. The formation energies of vacancy and <100> split-interstitial in diamonds were calculated to be 7.47 and 9.77 eV using our smoothly connected potential. These values agree well with the results of the reported first-principles calculations that the vacancy has a formation energy of 7.2 eV [45], and <100> interstitial has an energy of ∼10.23 eV [46]. Since nitrogen exists in diamond as a substituted atom, we calculated the substitutional formation energy of nitrogen to be 11.06 eV, well agreeing with the DFT results (ranging from 10.89–12.0 eV) [44]. In this study, these agreements prove the reliability and rationality of the fitted potential function.

2.2. Computational details

A large-scale atomic/molecular massively parallel simulator code was used to complete the MD simulations [15]. The size of the models is $60a_0 \times 60a_0 \times 60a_0$ ($a_0 = 3.567$ Å), containing 172, 800 and 0 carbon atoms, with the periodic boundary conditions. In these systems, 900 ppm of nitrogen impurity was randomly doped. It should be noted that these simulations involving 900 ppm nitrogen-doped diamond do not

correspond to experimental irradiation and annealing of such heavily-doped diamond crystals. The high nitrogen concentration was specifically chosen to facilitate the observation of NV center formation in the simulations since the formation of NV centers is influenced by the concentrations of both nitrogen and vacancy. In addition, 25 ppm of nitrogen was set in the central region because carbon vacancies were generated in the middle area by cascade collisions of the primary knock-on atom (PKA) atom, as depicted in figure S1(a) of the SI file. Thus, there is more nitrogen near vacancies produced by irradiation. In figure S1(b), the central atom of the model serves as the PKA atom during irradiation, which is incident from [111], [110] and [100] orientations with a 15 degree-inclination to avoid the channeling effects [47]. The MD study is divided into three parts, namely relaxation, irradiation process and annealing process. An irradiation energy of 5 keV and room temperature were used in the irradiation process. Afterwards, the models were annealed at 973, 1073 and 1173 K, respectively. The detailed calculation settings and temperature variations over time throughout the entire process are shown in figure S2 of the SI file. A total of 48 simulations was conducted in this study for each condition, as listed in table S1. The heating and cooling rates during the annealing process are both 1 K ps^{-1} and the holding time is 500 ps. An open visualization tool package was used to analyze and visualize the evolution of point defects [48]. The Frenkel pairs were identified by the Wigner–Seitz method [49].

Vienna *ab initio* simulation package software was used to perform first-principles calculations [50]. The Perdew–Burke–Ernzerhof [51] exchange with generalized gradient approximation correlation functions was used to optimize the basic diamond cell. The calculated lattice constant is 3.571 Å, which is consistent with the measured data (3.567 Å) [52]. We built a $4 \times 4 \times 4$ supercell with 512 atoms, with only the Γ-point considered. The force convergence value was 0.01 eV·Å^{-1} and the cutoff energy was 500 eV. To offer a more precise depiction of the VM process, we employed the climbing image nudged elastic band method [53]. The spring constant between the image states was designated a value of −5.0 eV Å^{-2} (the negative sign activating the nudging effect), a setting that was

empirically determined to have no effect on the maximum energy image state [53].

2.3. Experimental details

The adopted rough diamond sample was synthesized by Zhongnan Diamond Co., Ltd in a cubic press, under 1420–1720 K and 4.5–6.5 GPa, with Fe–Co–Ni catalyst and its nitrogen doping level at 10^{18} cm^{-3} order of magnitude. Experimental characteristics were performed on a slice cut from a high-pressure and high-temperature synthesized diamond. The slice ($2.74 \times 2.79 \times 1.12$ mm^3) was polished parallel to the cubic face to allow a clear view into the growth sectors {111}, {100} and some of the {110} [54] (as shown in figure S3(b)). It contains a nitrogen level of 18.5 ppm, determined based on the *in situ* Fourier transform infrared spectrometer spectra in figure S3 using an empirical formula as referenced in [16, 55–57]. Details of the calculations are displayed in the SI file. The sample was irradiated perpendicular to the {100} surface (i.e. along the [100] direction) with 10 MeV electrons at a fluence of 1.5×10^{17} cm^{-2} using a 20 kW cascade electron accelerator. The fluence rate is 6.8×10^{12} cm^{-2} s^{-1}. The temperature of the sample was controlled using a customized water-cooling unit, ensuring that the irradiation-induced increased temperature did not cause the water to boil, thereby preventing any occurrence of high-temperature annealing. The slice was then annealed for an hour at 1073 K in a Kejing GSL-1700X tube. A JASCO NRS7500 Raman spectrometer equipped with a Linkam THMS600 thermal stage was used to characterize the sample's photo-luminescence (PL) spectra excited by a 532 nm laser, before and after each step. The PL spectra are shown in figure S4, with peaks of NV^0, NV$^-$ and V^0 defects around 575, 637 and 741 nm, respectively. We conducted spatial mappings of NV^0, NV$^-$ and V^0 defects, with peaks at 575, 637 and 741 nm, respectively, over the slices in square regions (approx. 3×3 mm^2). The entire PL test was performed at ∼77 K.

3. Results and discussion

3.1. Migration of vacancies during annealing

A snapshot is presented in figure 2 to demonstrate three possible states of carbon atoms during the irradiation process using MD simulation. Detailed results are given in figure S5 in the SI file. The number of point defects generated by irradiation in diamond is dependent on the crystal orientation [58]. As shown in figure S5, the [111] and [100] directions generate a similar number of defects, with values of 38 and 36.8 ppm, respectively. In contrast, vacancy formation in the [110] direction is significantly lower, with a value of approximately 20 ppm. The evolution of Frenkel pairs in as-irradiated nitrogen-doped diamonds in figure S5 aligns with previous works [32, 58], signifying the suitability of the chosen potential. During irradiation, some of the carbon atoms move out of their initial lattice sites, leaving vacancies behind. Displaced carbon atoms will reach one of the three possible destinations,
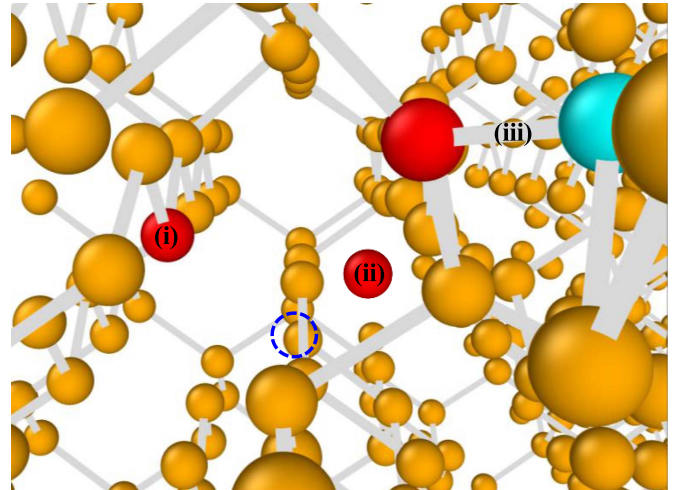

Figure 2. Three possible states of irradiated carbon atoms: (i) substitute another carbon atom (C$_{sub}$) site; (ii) interstitial (C$_i$) site; (iii) split-interstitial (C$_{split\text{-}i}$) site. Dashed blue circle represents the carbon vacancy site induced by irradiation.

depending on the moving distance: (i) substituting another lattice carbon atom (C$_{sub}$ site in figure 2(a)), (ii) becoming an interstitial atom (C$_i$ site in figure 2(b)) or (iii) joining with another interstitial carbon atom to form a <100> split-interstitial (C$_{split\text{-}i}$ site in figure 2(c)). When the proper temperature is reached, vacancies will interact with neighboring carbon atoms to initiate the VM process.

As characterized in the previous experimental researches [25, 26, 59], vacancies will migrate during the annealing process. Figure 3 shows the microscopic snapshots of annealing up to 1073 K (the animation can be viewed in the video 1). After irradiation, the B-atom transforms into a carbon interstitial, leaving a vacancy near the A-atom (depicted in figure 3(b)). Upon initiation of the annealing process, the A-atom migrates towards the vacancy and eventually reaches the B-site at the holding stage at 1110 ps, where the setting temperature is attained (figure S6(c)). Following a 30 ps interval of temperature maintenance, the A-atom successfully occupies the prior vacancy position (figure 3(d)). This state remains unchanged until the end of annealing. This reveals the typical process of vacancies migrating by exchanging positions with neighboring carbon atoms.

Furthermore, vacancies will experience multiple migration processes. For example, figure S7 shows that the microscopic process of vacancy migration is four times higher as the annealing time increases. The average migration distance between carbon vacancies in diamond is 1.67 Å, indicating that the vacancy is able to interchange with nearby carbon atoms stepwise, rather than by hopping. However, a more exceptional phenomenon is also observed, as shown in figure 4. After irradiation, the red atom (C-site) become C$_i$, while the A and B sites beside them become vacant positions (figure 4(a)). An important event occurs under the impact of annealing at 840 ps and 1042.8 K, where the red atom recombines into its initial position (figure 4(b)). Following that, at 860 ps and 1062.0 K,
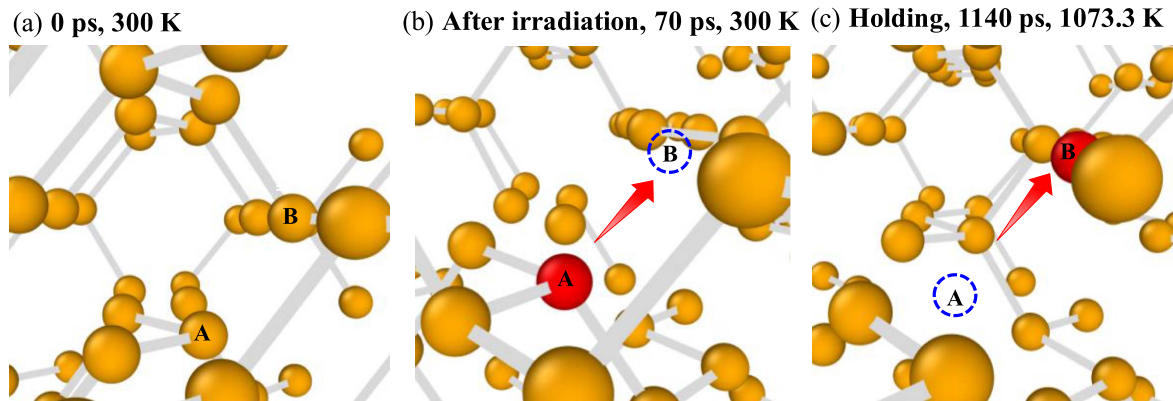
(a) **0 ps, 300 K** (b) **After irradiation, 70 ps, 300 K** (c) **Holding, 1140 ps, 1073.3 K**

Figure 3. (a)–(c) MD snapshots of a single vacancy migration during the irradiation and annealing processes in diamond. Vacancy site is represented by a dashed blue circle. Red arrow represents one carbon atom (at the A-site) progressively moving to the B-site as the increased temperature during annealing. Notably, the vacancy undergoes a positional shift from the B-site to the A-site.
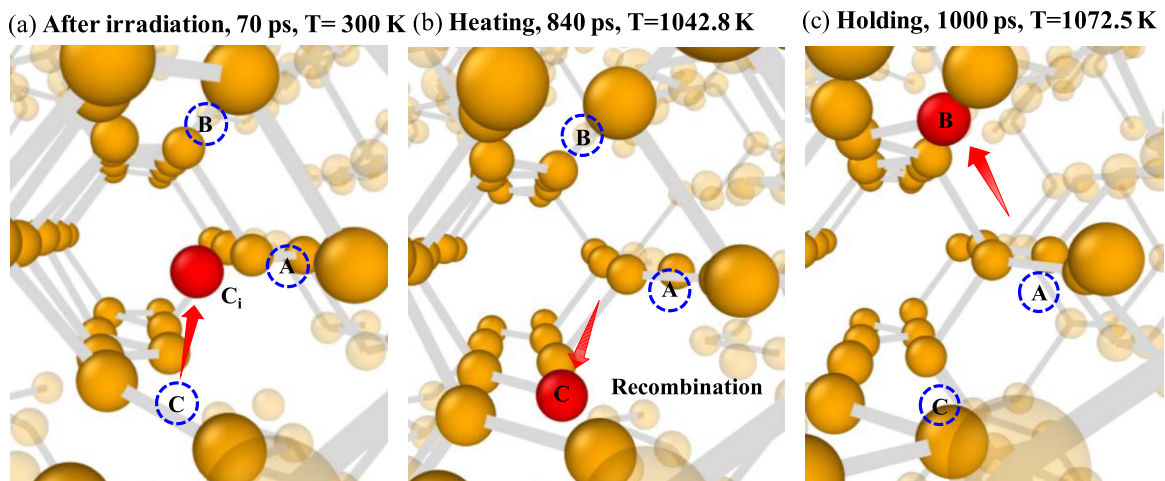
(a) **After irradiation, 70 ps, T= 300 K** (b) **Heating, 840 ps, T=1042.8 K** (c) **Holding, 1000 ps, T=1072.5 K**

Figure 4. (a)–(c) MD snapshots of an exceptional case of vacancy migration. Dashed blue circles represent vacancies. Red arrows represent the migration paths. During the annealing process, the red interstitial atom C_i in (a) is drawn back to its initial vacancy site in (b), but eventually moves to the A-vacancy site and (c) continues to move to the B-vacancy site with further annealing. Finally, the vacancy position shifts from (b) to (c).

the red atom migrates outwards, gradually approaching the B-site (figure 4(c)). As demonstrated by this example, with an additional vacancy nearby, the vacancy is more likely to migrate rather than recombine. Finally, a di-vacancy emerges in this case. A dynamic video and complete snapshots of this phenomenon can be found in the video 3 and figure S8, respectively.

3.2. Formation mechanisms of NV center

Based on the above observations, three mechanisms of NV center formation are proposed herein, as shown in figure 5, namely the INF, IFA to form NV, and VM to form NV. Figure 5(a) shows the detailed mechanism of the INF process. The carbon A-atom close to the nitrogen atom can be knocked out of the lattice site to form a $C_{\text{split-i}}$, leaving a vacancy near the nitrogen atom, and an NV center is formed after irradiation. In figure 5(b), which demonstrates the IFA

process, in which the A-atom is located near, but not totally at, another vacancy site (B-site) after irradiation, eventually settling into a C_i site. This NV center is unstable until the annealing temperature reaches 645.9 K. After annealing, the A-atom totally replaces the B-site, becoming a vacancy and forming the NV center with the nitrogen atom. The VM process is shown in figure 5(c). After irradiation, the C-site becomes a vacancy, and the A-atom and B-atom will migrate one by one, as described in the VM mechanism. That is, the vacancy migrates from C-site to A-site, forming the NV center with nitrogen. In this case, the vacancy starts to travel towards nitrogen at 1072.7 K. After migrating twice, the vacancy reaches an adjacent position by a nitrogen atom with a closest distance of 1.79 Å, as depicted in figure S9. These videos can be found in video 4–6.

To verify the reliability of the MD simulation results, irradiation experiments are conducted with a type-Ib diamond sample with a nitrogen concentration of 18.5 ppm, as shown
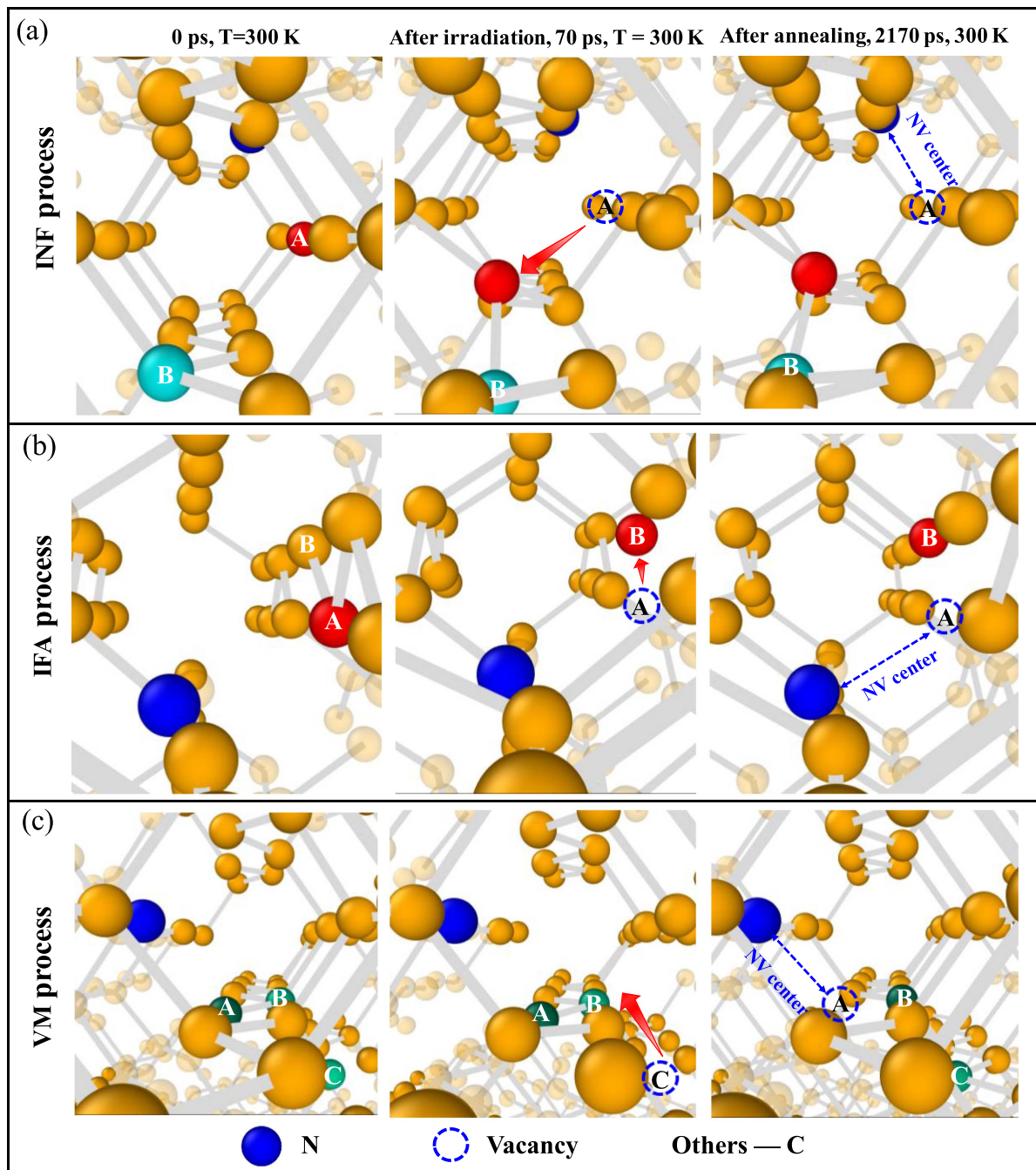
Figure 5. Three possible mechanisms of NV center formation. (a)INF, (b) IFA to form NV and (c) VM to form NV.

in figure 6. We show the optical images and PL mapping results of the diamond slice before irradiation, after irradiation and after further annealing. There is a block pattern that contains a distinct combination of {100}, {110} and {111} growth sectors (figure 6(a1)). These differences in growth sectors are related to the concentration of the substitutional nitrogen ($[N_0^s]$). The {110} sector has the lowest nitrogen concentration among the three sectors in the IR mapping results in figure S3(b) of the SI file. This feature provides insight into discussing the generation process of NV formation. After irradiation, the spatial distribution of the body color became more apparent (figure 6(b1)). NV^0, NV^- and V^0 centers at the PL

peak of 637, 575 and 741 nm were barely detected before irradiation (figures 6(a2)–(a4)), but obviously emerged after irradiation (figures 6(b2)–(b4)). NV^0 and NV^- centers with an intensity below 10^3 are found to be in greater abundance in the {111} and {100} regions than the {110} region for the lowest nitrogen content. This suggests that a considerable number of NV centers can be generated after irradiation, consistent with previous observations that NV centers can be formed after ultra-high energy (155 MeV) electron irradiation [18] and validates the first mechanism observed theoretically. The DFT calculation of Deák *et al* [30] also proved the result. To remove the carbon atoms attached to nitrogen, only three strong C–C
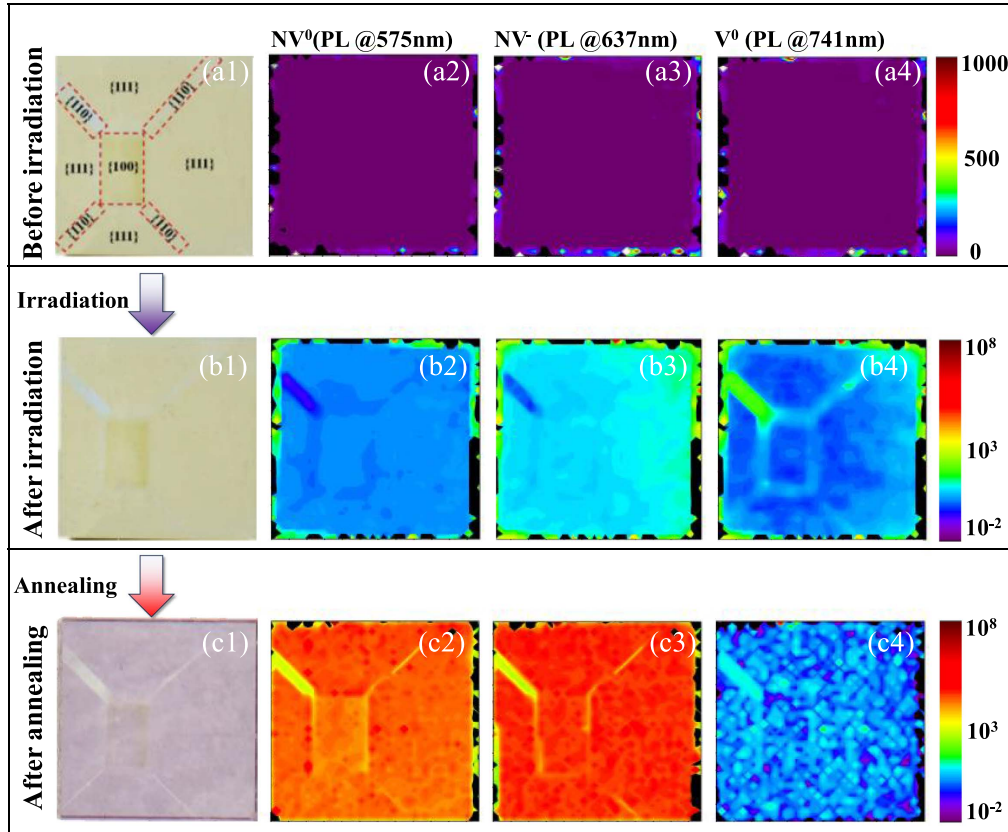
Figure 6. Characteristics for a type-Ib diamond sample (a1)–(a4) before irradiation, (b1)–(b4) after irradiation and (c1)–(c4) after further annealing. First column is the optical images and the other columns are PL peak mapping for NV^0, NV^- and V^0 signals. PL peak mapping of V^0 is obtained at 741 nm. Note that the PL mappings cover the whole diamond sample area (3 mm × 3 mm). Intensity scale in (a) ranges from 0–1000, while that in (b) and (c) ranges from 10^{-2} to 10^8.

bonds need to be broken, whereas in a perfect diamond lattice, four such bonds must be broken to create an isolated vacancy. This large energy difference results in a strong tendency to produce NVs even during non-equilibrium irradiation processes, which also shows the reasonability of MD simulations. Furthermore, in the {110} sector, there is less nitrogen, resulting in a higher presence of vacancy defects, identified as the V^0 center (figure 6(b4)).

Figures 6(c2)–(c4) illustrate a significant increase in NV^0 and NV^- intensity after annealing, with NV^- intensity reaching approximately 10^7 in the {111} and {100} regions. In addition, there is a marked increase in the NV center signal in the {110} region, indicating that annealing indeed serves as a key driver for the emergence of NV centers, which aligns with experimental conclusions [21–23, 27, 28]. Concurrently, in figures 6(c2) and (c3), the signal intensity of the NV center in the {110} area stands at a mere 10^3, while V^0 exhibits a stronger signal than the other two areas. This suggests that V^0 cannot be entirely exhausted due to nitrogen concentration constraints. This involves the distribution of nitrogen concentrations, which is beyond the scope of this article. Typically, the diamond sample's nitrogen level stands at 18.5 ppm, diverging from the simulation levels. However, the experiment confirms its alignment with our theoretical model even at minimal nitrogen levels, affirming the universality of

our simulation findings. This offers a conceptual framework for the controllable preparation of NV centers in diamond samples that possess minimal nitrogen levels.

Both mechanisms, being the second and third ones, involve processes related to annealing. We calculate the energy barrier of continuous VM towards nitrogen using first-principles calculations based on MD observations. To examine the energetic restrictions that govern VM, we designed two distinct pathways, namely Path I and Path II, as depicted in figure 7. Each pathway provides insight into the energy barriers of the process. Note that Path I is composed of two sub-paths. In Path I, the vacancy follows the direction of the chemical bond, starting from the distal site and eventually converging at the proximal site to form an NV center. This serves to demonstrate that the proximity of the vacancy to nitrogen reduces the energy barrier, making it easier to generate an NV center. The energy barrier associated with Path Ia is 2.76 eV (figure 7(b)), which is consistent with previously reported calculations of a VM energy barrier of 2.80 eV in diamond without nitrogen impurities [60]. These findings imply that the incorporation of nitrogen atoms into the crystal lattice has little effect on the energy required for VM. However, when the vacancy migrates to a position immediately adjacent to the nitrogen atom (Path Ib) to form an NV center, the influence of the nitrogen atom becomes evident with an energy barrier of only 0.71 eV.
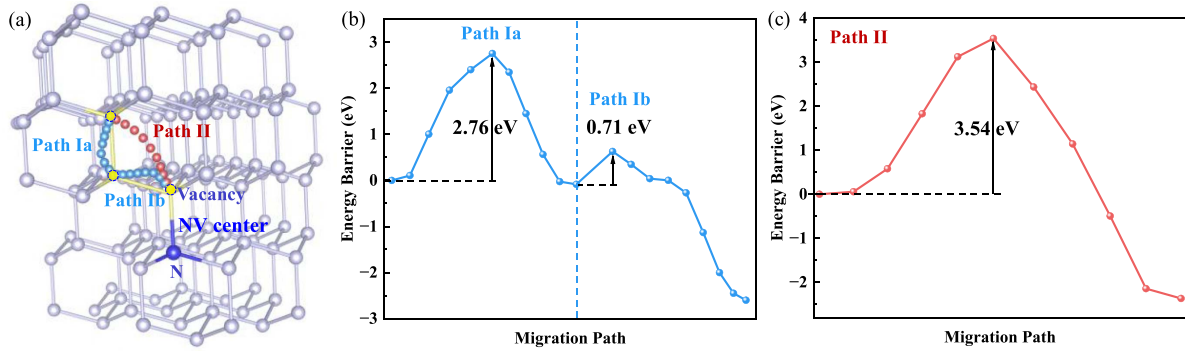
Figure 7. (a) Paths of vacancy (blue circle) migration towards the nitrogen atom to form an NV center by first-principles calculation. Cyan balls and red balls represent the migration snapshots along Path I and Path II, respectively. (b) Migration energy barrier of Path Ia and Ib. (c) Migration energy barrier of Path II.
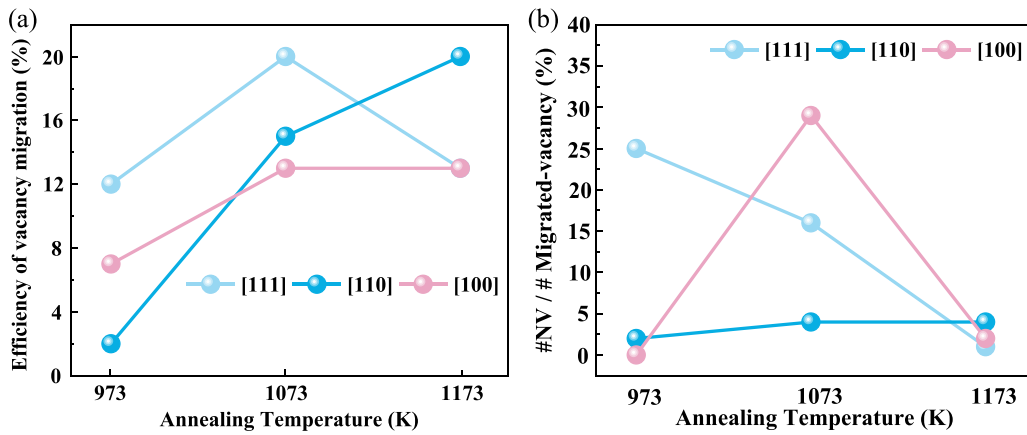

Figure 8. (a) Efficiency of vacancy migration and (b) the ratio of #NV/#migrated-vacancy at different annealing temperatures. # symbol represents the corresponding number.

Conversely, in the second scenario, referred to as Path II, the vacancy migrates directly towards nitrogen in a hopping motion, immediately settling close to the nitrogen atom, thereby creating the NV center. A significantly higher energy barrier of 3.54 eV is shown in figure 7(c). Our MD simulations indicate that the distance between the isolated nitrogen and the vacancy is negatively correlated with the vacancy's migration energy. If irradiation creates vacancies too far away from the nitrogen atoms, it may be difficult to move next to nitrogen. This increased energy requirement implies that during the formation of NV centers, the vacancy tends to migrate along virtual chemical bonds present in the diamond crystal lattice rather than directly towards the neighboring nitrogen atom. The experiment in figure 6 demonstrates that after annealing, numerous NV^0 and NV^- centers appear in diamond, indicating that many vacancies migrate to promote the formation of NV centers during the annealing process. These results elucidate the mechanism of VM and post-irradiation annealing to generate NV centers.

3.3. Effects of annealing temperature

The effects of annealing temperature on the VM and NV center formation were explored using MD statistics, as depicted in figure 8. The results demonstrate that the average migration temperature of the vacancy is 939.2 K, aligning with previous findings that suggest that VM occurs within a temperature range of 873–1173 K [22, 23, 25–28, 61]. According to the experimental results, NV centers form most easily at around 1073 K [22, 61], and the yield increases by 1.8 times when the diamond is annealed after low-energy electron irradiation at 800 °C (about 1073 K) [62]. As shown in figure 8(a), the VM efficiency at 973, 1073 and 1173 K is 12%, 20% and 13%, respectively, for the [111] orientation, 7%, 13% and 13%, respectively, for the [100] direction and 2%, 15% and 20%, respectively, for the [110] direction. It is revealed that 1073 K is the most suitable temperature for forming NV centers along [111] and [100] directions with little difference observed between 1073 and 1173 K for the [100] direction. In contrast, for the [110] orientation, higher temperatures promote VM.

In terms of the ratio of NV centers to migrated vacancies (#NV/#migrated-vacancy) in figure 8(b), the [111] direction has the highest formation rate at 973 K, whereas 1073 K is most beneficial for the production of NV centers along the [100] direction. Regarding the [100] direction, the number of NV centers formed under 1073 K is 29 times that of 973 K and 14 times that of 1173 K. In the [110] direction, 973 K is

less conducive to the formation of NV centers, while the number of NV centers at 1073 K is similar to that at 1173 K. This observation corresponds with the results of vacancy migration time at different annealing temperatures shown in figure S11. The above results show that higher annealing temperature does not guarantee a higher formation rate of NV centers, which is also dependent on crystallographic direction. Thus, the annealing temperature needs to be selected on a case-by-case basis.

Simulation results further reveal that VM and NV formation is orientation-dependent. The differences in VM and NV center formations across different orientations were analyzed using MD simulations, as presented in figure S11. The minimum migration temperatures in the [111], [110]and [100] directions are 613.6, 700.5 and 531.8 K, respectively, following the trend [110] > [111] > [100]. A previous experiment shows that vacancies can diffuse within a short range at 773 K in type-Ib diamond with high nitrogen concentrations [63]. Our simulation results suggest that the temperature at which VM occurs varies widely and depends on the crystallographic direction. Given that the [110] direction yields the fewest vacancies (figure S5) and necessitates the highest annealing temperature (figure S10) for VM, forming NV centers in this direction proves to be the most challenging. In addition, in figure S11(b), even though the [111] direction has the strongest potential to form an NV center through VM, the NV center's ratio to total vacancies is less than that of the [100] direction. A possible explanation is that vacancies in the [111] direction have a higher probability of creating a double vacancy than those in the [100] direction, leading to a reduced number of vacancies for establishing an NV center due to the formation of double vacancy defects.

4. Conclusion

In summary, the mechanism of NV center formation via an irradiation and annealing approach in type-Ib diamond has been demonstrated through MD simulations, first-principles calculations and experiments. Three formation strategies of NV centers are identified: INF, IFA to form NV, and VM to form NV. Our simulations reveal that VM occurs via a stepwise interchange with nearby carbon atoms at proper temperatures. The threshold annealing temperature for VM depends on the orientation, with average values of 613.6, 700.5 and 531.8 K along the [111], [110] and [100] directions, respectively. It is important to note that a higher annealing temperature does not guarantee a higher yield of NV center formation since it also depends on the crystallographic orientation. This study provides valuable insight into the formation mechanism and further controllable preparation of NV centers.

5. Future perspectives

In this study, we have successfully revealed the atomic-level formation mechanism of the NV center in type-Ib diamond, prepared by irradiation and annealing, from a multi-scale perspective. We combine MD simulations, first principles calculations and experimental verification to systematically clarify

the key processes of NV center preparation, demonstrating the potential for achieving controlled preparation of NV centers. In addition, the NV center is closely dependent on the crystallographic orientation of diamond, indicating that it is useful to regulate the concentration of NV centers according to the characteristics of the orientation. Critical theoretical foundation and strategy are provided for the more precise, controllable and quantitative preparation of NV centers at the atomic level to reduce the complexity and high cost of experiments. Looking into the future, the widespread application of NV centers will increasingly depend on the precise control of their preparation process. Further research is warranted to address challenges, such as controllability, stability and quality, from a cross-scale perspective. Using the proposed models and methods, we can thoroughly explore the optimization of irradiation annealing, ion implantation and other processes. As we continue to optimize and improve the controlled preparation process of NV centers, we expect to promote the progress of NV centers in quantum science and industrial applications in the future.

Acknowledgments

Conflict of interest

The authors declare that they have no known competing financial interests or personal relationships that could have appeared to influence the work reported in this paper.

Author contributions

Taiqiao Liu: Conceptualization, Investigation, Methodology, Data curation, Writing–original draft. **Fanglin Lyu:** Experiments, Writing-review & editing. **Tian Shao:** Experiments. **Diwei Zou:** Data curation. **Wei Shen:** Supervision, Resources, Software. **Yuzheng Guo:** Software.

Yuan Zhong: Data curation. **Chaoyang Chen:** Methodology. **Liangchen Yi:** Resources. **Zhaofu Zhang:** Supervision, Conceptualization, Resources, Project administration, Writing–review and editing. **Andy H Shen:** Supervision, Resources, Writing–review and editing, Project administration, Funding acquisition.

ORCID iD

Zhaofu Zhang ⓘ https://orcid.org/0000-0002-1406-1256

References

[1] Gruber A, Dräbenstedt A, Tietz C, Fleury L, Wrachtrup J and Borczyskowski C V 1997 Scanning confocal optical microscopy and magnetic resonance on single defect centers *Science* **276** 2012–4

[2] Shen W, Wu G, Li L, Li H, Liu S, Shen S and Zou D 2022 Fluorine-terminated diamond (110) surfaces for nitrogen-vacancy quantum sensors *Carbon* **193** 17–25

[3] Wang Z, Kong F, Zhao P, Huang Z, Yu P, Wang Y, Shi F and Du J 2022 Picotesla magnetometry of microwave fields with diamond sensors *Sci. Adv.* **8** eabq8158

[4] Prawer S and Greentree A D 2008 Diamond for quantum computing *Science* **320** 1601–2

[5] Shen W, Shen S, Liu S, Li H, Zhang Y, Zhang Q and Guo Y 2021 Epoxy oxidized diamond (111)-(2 × 1) surface for nitrogen-vacancy based quantum sensors *Carbon* **173** 485–92

[6] Chang Y R *et al* 2008 Mass production and dynamic imaging of fluorescent nanodiamonds *Nat. Nanotechnol.* **3** 284–8

[7] Wu Y and Weil T 2022 Recent developments of nanodiamond quantum sensors for biological applications *Adv. Sci.* **9** 2200059

[8] Kucsko G, Maurer P C, Yao N Y, Kubo M, Noh H J, Lo P K, Park H and Lukin M D 2013 Nanometre-scale thermometry in a living cell *Nature* **500** 54–58

[9] Wang J *et al* 2015 High-sensitivity temperature sensing using an implanted single nitrogen-vacancy center array in diamond *Phys. Rev.* B **91** 155404

[10] Taylor J M, Cappellaro P, Childress L, Jiang L, Budker D, Hemmer P R, Yacoby A, Walsworth R and Lukin M D 2008 High-sensitivity diamond magnetometer with nanoscale resolution *Nat. Phys.* **4** 810–6

[11] Yip K Y *et al* 2019 Measuring magnetic field texture in correlated electron systems under extreme conditions *Science* **366** 1355–9

[12] Pham L M *et al* 2016 NMR technique for determining the depth of shallow nitrogen-vacancy centers in diamond *Phys. Rev.* B **93** 045425

[13] Watanabe A, Nishikawa T, Kato H, Fujie M, Fujiwara M, Makino T, Yamasaki S, Herbschleb E D and Mizuochi N 2021 Shallow NV centers augmented by exploiting n-type diamond *Carbon* **178** 294–300

[14] Staudacher T, Raatz N, Pezzagna S, Meijer J, Reinhard F, Meriles C A and Wrachtrup J 2015 Probing molecular dynamics at the nanoscale via an individual paramagnetic centre *Nat. Commun.* **6** 8527

[15] Yu S J, Kang M W, Chang H C, Chen K-M and Yu Y-C 2005 Bright fluorescent nanodiamonds: no photobleaching and low cytotoxicity *J. Am. Chem. Soc.* **127** 17604–5

[16] Su L J, Fang C Y, Chang Y T, Chen K M, Yu Y C, Hsu J H and Chang H C 2013 Creation of high density ensembles of nitrogen-vacancy centers in nitrogen-rich type Ib nanodiamonds *Nanotechnology* **24** 315702

[17] Jaffe T *et al* 2020 Novel ultra localized and dense nitrogen delta-doping in diamond for advanced quantum sensing *Nano Lett.* **20** 3192–8

[18] Losero E, Goblot V, Zhu Y, Babashah H, Boureau V, Burkart F and Galland C 2023 Creation of NV centers in diamond under 155 MeV electron irradiation *J. Adv. Phys.* **3** 2300071

[19] Orwa J O *et al* 2011 Engineering of nitrogen-vacancy color centers in high purity diamond by ion implantation and annealing *J. Appl. Phys.* **109** 083530

[20] Liu Y, Chen G, Song M, Ci X, Wu B, Wu E and Zeng H 2013 Fabrication of nitrogen vacancy color centers by femtosecond pulse laser illumination *Opt. Express* **21** 12843–8

[21] Capelli M, Heffernan A H, Ohshima T, Abe H, Jeske J, Hope A, Greentree A D, Reineck P and Gibson B C 2019 Increased nitrogen-vacancy centre creation yield in diamond through electron beam irradiation at high temperature *Carbon* **143** 714–9

[22] Tallaire A *et al* 2020 High NV density in a pink CVD diamond grown with N_2O addition *Carbon* **170** 421–9

[23] Kollarics S *et al* 2022 Ultrahigh nitrogen-vacancy center concentration in diamond *Carbon* **188** 393–400

[24] Botsoa J, Sauvage T, Adam M P, Desgardin P, Leoni E, Courtois B, Treussart F and Barthe M-F 2011 Optimal conditions for NV⁻ center formation in type-Ib diamond studied using photoluminescence and positron annihilation spectroscopies *Phys. Rev.* B **84** 125209

[25] Dobrinets I A, Victor V G and Zaitsev A M 2016 HPHT-treated diamonds *Series in Materials Science* vol 181 (Springer) pp 59–73

[26] Sally E M, Ardon T, Smit K V, Breeding C M and Shigley J E 2019 Natural-color pink, purple, red, and brown diamonds: band of many colors *Gems Gemol.* **54** 320–37

[27] Wang K, Guo R, Zhang Y and Tian Y 2020 Photoluminescence and annealing of nitrogen-interstitials defects in electron irradiated diamond *Spectrosc. Lett.* **53** 1–7

[28] He J, Liu J, Xiu Q, Sun Z, Kang A and Zheng Y 2022 Effect of irradiation and annealing on the nitrogen vacancy color center yield of diamond *Acta Opt. Sin.* **42** 128–35

[29] Mainwood A 1994 Nitrogen and nitrogen-vacancy complexes and their formation in diamond *Phys. Rev.* B **49** 7934–40

[30] Deák P, Aradi B, Kaviani M, Frauenheim T and Gali A 2014 Formation of NV centers in diamond: a theoretical study based on calculated transitions and migration of nitrogen and vacancy related defects *Phys. Rev.* B **89** 075203

[31] Adler J, Silverman A, Ierushalmi N, Sorkin A and Kalish R 2014 Simulation and visualization of ion-implantation in diamond *J. Phys.: Condens. Matter* **487** 012015

[32] Buchan J T, Robinson M, Christie H J, Roach D L, Ross D K and Marks N A 2015 Molecular dynamics simulation of radiation damage cascades in diamond *J. Appl. Phys.* **117** 245901

[33] Smith R 1990 A classical dynamics study of carbon bombardment of graphite and diamond *Proc. R. Soc.* A **431** 143–55

[34] Saada D, Adler J and Kalish R 1999 Computer simulation of damage in diamond due to ion impact and its annealing *Phys. Rev.* B **59** 6650–60

[35] Ran Q, Zhou Y, Zou Y, Wang J, Duan Z, Sun Z, Fu B and Gao S 2021 Molecular dynamics simulation of displacement cascades in cubic silicon carbide *Nucl. Mater. Energy* **27** 100957

[36] Biersack J P and Ziegler J F 1985 The stopping and range of ions in matter *Treatise on Heavy-Ion Science* ed D A Bromley (Springer) (https://doi.org/10.1126/science.228.4701.858)

[37] Devanathan R, Rubia T and Weber W J 1998 Displacement threshold energies in β-SiC *J. Nucl. Mater.* **253** 47–52

[38] Zhao W, Xu Z, Ren F, Dong B, Zhao J and Wang P 2023 Enhancing the fabrication yield of NV centers in diamond by pre-doping using molecular dynamics simulation *Diamond Relat. Mater.* **132** 109683

[39] Lehtinen O, Naydenov B, Börner P, Melentjevic K, Müller C, McGuinness L P, Pezzagna S, Meijer J, Kaiser U and Jelezko F 2016 Molecular dynamics simulations of shallow nitrogen and silicon implantation into diamond *Phys. Rev. B* **93** 035202

[40] Matsunaga K, Fisher C and Matsubara H 2000 Tersoff potential parameters for simulating cubic boron carbonitrides *Jpn. J. Appl. Phys.* **39** L48

[41] Dasmahapatra A and Kroll P 2018 Modeling amorphous silicon nitride: a comparative study of empirical potentials *Comput. Mater. Sci.* **148** 165–75

[42] Los J H, Kroes J M H, Albe K, Gordillo R M, Katsnelson M I and Fasolino A 2017 Extended tersoff potential for boron nitride: energetics and elastic properties of pristine and defective h-BN *Phys. Rev. B* **96** 184108

[43] Zhao S, Xiong Y, Ma S, Zhang J, Xu B and Kai J-J 2021 Defect accumulation and evolution in refractory multi-principal element alloys *Acta Mater.* **219** 117233

[44] Sholihun S, Kadarisman H P and Nurwantoro P 2018 Density-functional-theory calculations of formation energy of the nitrogen-doped diamond *Indones. J. Chem.* **18** 749–54

[45] Bernholc J, Antonelli A, Del Sole T M, Bar-Yam Y and Pantelides S T 1988 Mechanism of self-diffusion in diamond *Phys. Rev. Lett.* **61** 2689–92

[46] Salustro S, Erba A, Zicovich-Wilson C M, Nöel Y, Maschio L and Dovesi R 2016 Infrared and Raman spectroscopic features of the self-interstitial defect in diamond from exact-exchange hybrid DFT calculations *Phys. Chem. Chem. Phys.* **18** 21288–95

[47] Lehtinen O, Naydenov B, Börner P, Melentjevic K and Jelezko F 2016 Molecular dynamics simulations of shallow nitrogen and silicon implantation into diamond *Phys. Rev. B* **93** 035202

[48] Stukowski A 2009 Visualization and analysis of atomistic simulation data with OVITO–the open visualization tool *Model. Simul. Mater. Sci. Eng.* **18** 015012

[49] Kettle S F A and Norrby L J 1994 The Wigner-Seitz unit cell *J. Chem. Educ.* **71** 1003

[50] Kresse G and Furthmüller J 1996 Efficient iterative schemes for ab initio total-energy calculations using a plane-wave basis set *Phys. Rev. B* **54** 11169

[51] Perdew J P, Burke K and Ernzerhof M 1996 Generalized gradient approximation made simple *Phys. Rev. Lett.* **77** 3865

[52] Warren J, Yarnell J, Dolling G and Cowley R 1967 Lattice dynamics of diamond *Phys. Rev.* **158** 805

[53] Henkelman G, Uberuaga B P and Jónsson H 2000 A climbing image nudged elastic band method for finding saddle points and minimum energy paths *J. Chem. Phys.* **113** 9901–4

[54] Burns R C, Cvetkovic V, Dodge C N, Evans D J F, Rooney M L T, Spear P M and Welbourn C M 1990 Growth-sector dependence of optical features in large synthetic diamonds *J. Cryst. Growth* **104** 257–79

[55] Lawson S C, Fisher D, Hunt D C and Newton M E 1998 On the existence of positively charged single-substitutional nitrogen in diamond *J. Phys.* **10** 6171–80

[56] Kiflawi I, Mayer A, Spear P, van Wyk J and Woods G 1994 Infrared absorption by the single nitrogen and A defect centres in diamond *Phil. Mag. B* **69** 1141–7

[57] Wang W H, Fang C, Chen L C, Zhang Z F, Zhang Y W, Wang Q Q, Wan B, Yang X, Ren W and Jia X P 2024 Effect of Fe_6N_2 on diamond growth under high pressure and high temperature conditions *Diamond Relat. Mater.* **142** 110863

[58] Liu T, Shao T, Lyu F, Lai X and Shen A H 2022 Molecular dynamics simulations to assess the radiation resistance of different crystal orientations of diamond under neutron irradiation *Model. Simul. Mater. Sci. Eng.* **30** 035005

[59] Räcke P, Pietzonka L, Meijer J, Spemann D and Wunderlich R 2021 Vacancy diffusion and nitrogen-vacancy center formation near the diamond surface *Appl. Phys. Lett.* **118** 204003

[60] Breuer S and Briddon P 1995 Ab initio investigation of the native defects in diamond and self-diffusion *Phys. Rev. B* **51** 6984

[61] Davies G J and Hamer M F 1976 Optical studies of the 1.945 eV vibronic band in diamond *Proc. R. Soc. A* **348** 285–98

[62] Schwartz J, Aloni S, Ogletree D F and Schenkel T 2012 Effects of low-energy electron irradiation on formation of nitrogen-vacancy centers in single-crystal diamond *New J. Phys.* **14** 043024

[63] Steeds J W and Kohn S 2014 Annealing of electron radiation damage in a wide range of Ib and IIa diamond samples *Diamond Relat. Mater.* **50** 110–22